Published in final edited form as:
J Am Chem Soc. 2008 December 17; 130(50): 17075–17084. doi:10.1021/ja8068177.

Targeting Inactive Enzyme Conformation:

Aryl Diketoacid Derivatives as a New Class of PTP1B Inhibitors

Sijiu Liu[#], **Li-Fan Zeng**[‖], **Li Wu**[#], **Xiao Yu**[#], **Ting Xue**[‖], **Andrea M. Gunawan**[‡], **Long Ya-Qiu**[‖,*], and **Zhong-Yin Zhang**[#,‡,*]

#Department of Biochemistry and Molecular Biology, Indiana University School of Medicine, 635 Barnhill Drive, Indianapolis, IN 46202, USA

‡*Chemical Genomics Core Facility, Indiana University School of Medicine, 635 Barnhill Drive, Indianapolis, IN 46202, USA*

‖*State Key Laboratory of Drug Research, Shanghai Institute of Materia Medica, Chinese Academy of Sciences, 555 Zuchongzhi Road, Shanghai 201203, China*

Abstract

There has been considerable interest in protein tyrosine phosphatase 1B (PTP1B) as a therapeutic target for diabetes, obesity, as well as cancer. Identifying inhibitory compounds with good bioavailability is a major challenge of drug discovery programs targeted toward PTPs. Most current PTP active site-directed pharmacophores are negatively charged pTyr mimetics which cannot readily enter the cell. This lack of cell permeability limits the utility of such compounds in signaling studies and further therapeutic development. We identify aryl diketoacids as novel pTyr surrogates and show that neutral amide-linked aryl diketoacid dimers also exhibit excellent PTP inhibitory activity. Kinetic studies establish that these aryl diketoacid derivatives act as noncompetitive inhibitors of PTP1B. Crystal structures of ligand-bound PTP1B reveal that both the aryl diketoacid and its dimeric derivative bind PTP1B at the active site, albeit with distinct modes of interaction, in the catalytically inactive, WPD loop open conformation. Furthermore, dimeric aryl diketoacids are cell permeable and enhance insulin signaling in hepatoma cells, suggesting that targeting the inactive conformation may provide a unique opportunity for creating active site-directed PTP1B inhibitors with improved pharmacological properties.

Introduction

Protein tyrosine phosphatases (PTPs) constitute a large family of enzymes, which are crucial modulators of tyrosine phosphorylation-dependent cellular events.[1] Malfunction in PTP activity is associated with many human diseases, including cancer, diabetes/obesity, and autoimmune disorders.[2] Among members of the PTP superfamily, PTP1B is considered one of the best-validated targets for therapeutic development. Biochemical and genetic evidence indicate that PTP1B plays a key role in regulating body weight, glucose homeostasis, and energy expenditure by acting as a key negative regulator of insulin and leptin receptor mediated signaling pathways. PTP1B-deficient mice display increased insulin sensitivity and improved glycemic control, and are resistant to diet-induced obesity.[3,4] Moreover, studies with PTP1B antisense oligonucleotides in diabetes animal models demonstrate that a reduction in PTP1B leads to decreases in adipose tissue mass, plasma insulin, and blood glucose levels.[5] These

*To whom correspondence should be addressed. E-mail: zyzhang@iupui.edu, and yqlong@mail.shcnc.ac.cn.

Data deposition: The coordinates for the structures of the PTP1B•LZP25 complex (accession number 3EB1), and the PTP1B•LZP6 complex (accession number 3EAX) have been deposited in the Protein Data Bank.

findings suggest that inhibition of PTP1B represents an effective strategy to combat metabolic syndromes such as type 2 diabetes and obesity.

Besides having a role in dampening insulin- and leptin-mediated processes, PTP1B also augments signaling downstream of growth factor receptors and integrins. To that end, PTP1B can remove the inhibitory phosphate from the C-terminus of Src, thereby promoting Src kinase activation.[6-8] In addition, PTP1B dephosphorylates the scaffolding adapter protein $p62^{DOK}$, leading to activation of the Ras-ERK pathway.[9] Given that PTP1B is capable of promoting both the Src kinase and Ras/Erk pathways, which are major components in HER2/*Neu* signaling, PTP1B may function as an oncogene in the context of breast cancer. Interestingly, PTP1B is up-regulated in HER2/*Neu*-transformed cells[10] and 90% of all breast tumors overexpress both HER2/*Neu* and PTP1B.[11] More recent studies reveal that crossbreeding transgenic mice expressing activated HER2/*Neu* with $PTP1B^{-/-}$ mice caused delayed HER2/*Neu*—induced mammary tumor development and reduced the incidence of lung metastases.[12,13] These data suggest that PTP1B-specific inhibitors may qualify as an effective treatment for breast cancer.

Given the compelling evidence linking PTP1B to multiple human diseases, major efforts have been initiated by both the pharmaceutical industry and academia to target PTP1B for therapeutic development. Contrary to the widely-held belief that PTPs are challenging targets for small molecule inhibitor development, numerous potent and selective PTP1B inhibitors have been described.[14] However, most of the reported compounds contain negatively charged nonhydrolyzable phosphotyrosine (pTyr) mimetics, due primarily to the highly positively charged nature of the active site evolved to bind pTyr. Consequently, poor membrane permeability has limited further advancement of such compounds as drug candidates. Thus, one challenge which has previously delayed realization of PTP1B-based small molecule therapeutics has been the identification of novel chemical entities with improved physicochemical properties and bioavailability.

We report the characterization of aryl diketoacids as novel pTyr surrogates for PTP inhibitor development. Surprisingly, we discovered that amide-linked aryl diketoacid dimers, which lack any formal charge, also exhibit PTP inhibitory activity. X-ray crystallographic analyses of ligand-bound PTP1B structures revealed that although monomeric and dimeric aryl diketoacid occupy and interact with the enzyme active site in distinct manner, both compounds stabilize PTP1B in its inactive, WPD loop open conformation. Importantly, dimeric aryl diketoacids are cell permeable and enhance insulin signaling in hepatoma cells. These properties suggest that it is possible to develop uncharged PTP1B active site-directed inhibitors with improved *in vivo* efficacy, thereby facilitating the development of PTP1B-based therapeutics for the treatment of diabetes, obesity, and breast cancer. Furthermore, targeting the inactive conformation may constitute a general strategy for PTP inhibitor design.

Materials and Methods

Materials

Polyethylene glycol (PEG) and buffers for crystallization were purchased from Hampton Research Co. *p*-Nitrophenyl phosphate (*p*NPP) was purchased from Fluke Co. Dithiothreitol (DTT) was provided by Fisher (Fair Lawn, NJ). Dulbecco's modified Eagle's medium (DMEM) and fetal bovine serum were purchased from ATCC. All of other chemicals and reagents were of the highest commercially available grade. Polyclonal insulin receptor β-subunit dual-phospho-specific (pY1162/pY1163) antibody was purchased from BioSource International (Camarillo, CA). Human insulin, sodium orthovanadate, iodoacetic acid (IAA) and Nonidet P-40 were from Sigma (St. Louis, MO).

Synthesis of Aryl Diketoacid Derivatives[15,16]

To a stirred mixture of *tert*-BuONa (2.5 equiv) and dimethyl oxalate (2.0 equiv) in anhydrous THF at 0°C was added dropwise aryl methyl ketone (1.0 equiv) in DME. The resulting orange-yellow mixture was stirred at room temperature for a maximum of 1.5 h. The reaction was quenched with a 1.0 M HCl aqueous solution and the compound was extracted with CH_2Cl_2. The combined organic layers were washed with saturated aqueous $NaHCO_3$ and brine, respectively, dried over anhydrous Na_2SO_4 and concentrated under vacuum. Purification by silica gel flash chromatography provided the desired *m*/*o*/*p*-substituted phenyl-4-oxo-2-hydroxy-2-butenoic acid methyl ester. Subsequent hydrolysis of the resulting aryl diketoacid methyl ester readily furnished the corresponding aryl diketoacid by 1 N NaOH in MeOH-THF (1:1) at room temperature. Synthesis and physicochemical data of the compounds LZP3-4, LZP6-9 and LZP37-38 were reported previously.[17,18]

4-(3-(Dibenzylamino)phenyl)-2,4-dioxobutanoic acid (LZP25)

Yellow powder, yield 89%. ^{1}H NMR (300 MHz, $CDCl_3$): δ 7.27-7.24 (m, 14H), 4.68 (s, 4H). EI-MS (*m*/*z*): $(M-72)^+$. Analytical RP-HPLC t_R = 11.1 min (gradient 30-90% of solvent C over 20 min, purity 100%), t_R = 9.2 min (gradient 30-90% of solvent B over 20 min, purity 100%).

2,4-dioxo-4-phenylbutanoic acid (LZP-36)

Yellow solid, yield 90%. ^{1}H NMR (400 MHz, $CDCl_3$): δ 8.03-7.99 (m, 2H), 7.67-7.61 (m, 1H), 7.55-7.50 (m, 2H), 7.18 (s, 1H); EI-MS (*m*/*z*): 192 (M^+).

2,4-Dioxo-4-(4-(trifluoromethyl)phenyl)butanoic acid (LZP39)

White needle solid, yield 87.0%. ^{1}H NMR (400 MHz, $CDCl_3$): δ 8.11 (d, 2H, *J* = 8.0 Hz); 7.82 (d, 2H, *J* = 8.0 Hz); 7.20 (s, 1H). EI-MS (*m*/*z*, %): 260 (M^+, 3.0); 241 (4.0); 215 (100.0); 173 (45.0); 145 (37.0). HR-EIMS calcd for $C_{11}H_7F_3O_4$: 260.0296, found: 260.0301. Anal. Calcd for $C_{11}H_7F_3O_4 \cdot 0.2CH_2Cl_2 \cdot 0.8CH_3OH$: C 47.60, H 3.53; Found C 47.33, H 3.34.

1,1′-(Piperazine-1,4-diyl)bis(4-(3-(dibenzylamino)phenyl)butane-1,2,4-trione) (LZP40)

A drop of DMF was added to a turbid solution of 1.0 eq of LZP25 dissolved in 10 mL of dichloromethane at 0°C. Next, 1mL of $SOCl_2$ was added to the solution. The reaction mixture was stirred for 2 hours at room temperature, after which the solution was condensed in vaccum. The residue was dissolved in 10 mL of dichloromethane followed by addition of 0.5 eq of piperazine and a drop of pyridine. This solution was stirred for another 2 hours. Work up and dried by anhydrous sodium sulfate. Purification from chromatography (CH_2Cl_2/CH_3OH =20:1) gives LZP40 as light yellow solid in yield of 65%. ^{1}H NMR (300 MHz, $CDCl_3$): *δ* 7.36-7.31 (m, 10H), 7.28-7.24 (m, 10 H), 7.22 (m, 6H), 6.91 (d, 2H, *J* = 6.9Hz), 6.47 (s, 2H), 4.69 (s, 8H), 3.70 (m, 8H). ESI-MS *m*/*z*: calc. 824.9, found 823.2 $(M-1)^-$, 863.3 $(M+K)^+$. b.p. 105-106 °C. t_R = 25.6 min. (10-90% of solvent B over 28 min, purity 99%). t_R =24.1 min. (10-90% of solvent C over 24 min, purity 98%).

tert-Butyl 4-(4-(3-(benzyloxy)phenyl)-2,4-dioxobutanoyl) piperazine-1-carboxylate (LZP70)

A solution consisting of compound LZP4 (75 mg, 0.25 mmol), EDCI (73 mg, 0.38 mmol), DIPEA (66 μL, 0.38 mmol) and HOAt (51 mg, 0.38 mmol) in 10 mL of dry dichloromethane (1.5 mL) was stirred at room temperature for half an hour. To this solution was added *tert*-butyl piperazine-1-carboxylate (50 mg, 0.27 mmol) in dry THF. The reaction mixture was stirred for 12 h at room temperature and then poured into ice-water and extracted with dichloromethane. The combined organic layers were washed with water and brine and dried over anhydrous Na_2SO_4. The concentration provided the residue which was purified by chromatography using PE/EtOAc (1:1) as an eluent, which gives compound LZP70 as a brown

powder with a yield of 47%. ^{1}H NMR (300MHz, $CDCl_3$): δ 7.53 -7.37 (m, 8H), 7.17 (m, 1H), 6.58 (s, 1H), 5.11 (s, 2H), 3.66 (br, 4H), 3.51 (br, 4H), 1.47 (s, 9H); EI-MS (*m*/*z*): 466 (M^+).

tert-Butyl 4-(4-(3-(dibenzylamino)phenyl)-2,4-dioxobutanoyl) piperazine-1-carboxylate (LZP71)

LZP71 was prepared in a similar fashion as described for LZP70, resulting in a yellow solid with a yield of 50%. ^{1}H NMR (400MHz, $CDCl_3$): δ 7.36-7.21 (m, 13H); 6.93 (m, 1H); 6.44 (s, 1H); 4.69 (s, 4H), 3.62 (m, 4H), 3.48 (m, 4H); 1.47(s, 9H). EI-MS (*m*/*z*): 555 (M^+).

General Analytical Methods

Unless otherwise stated, the 1H NMR spectra were recorded on a Varian 300-MHz or 400-MHz spectrometer. Data are reported in parts per million relative to TMS and are referenced to the solvent. Elemental analyses were obtained using a Vario EL spectrometer. Melting points (uncorrected) were determined on a Buchi-510 capillary apparatus. IR spectra were recorded on Bio-Rad FTS-185 spectrometers. Mass spectrometry and HRMS (ESI) spectra were obtained on an APEXIII 7.0 T FTMS mass spectrometer. The degree of rotation was measured by P-1030 (A012360639) automatic polarimeter. Flash column chromatography was performed on silica gel H (10-40 μm). Anhydrous solvents were obtained using a standard procedure.

Analytical RP-HPLC was performed for selected compounds on two systems, using a Vydac C18 column (10 × 250 mm), monitored by a UV detector at 254 nm. Solvent gradient system 1, solvent A, 0.05% TFA in water; solvent B, 0.05% TFA in 90% acetonitrile in water; solvent gradient system 2, solvent A, 0.05% TFA in water; solvent C, 0.05% TFA in 90% methanol in water with a gradient over 20 min at a flow rate of 2.5 mL/min.

PTP1B

The catalytic domain of PTP1B (residues 1–321) and its mutants were expressed in *Escherichia coli* and purified to homogeneity as described previously.[19] All mutant forms of PTP1B were generated using the QuickChange kit from Stratagene.

Kinetic Analysis of PTP1B Inhibition by Aryl Diketoacids and Their Dimers

Compounds were dissolved in DMSO to a concentration of 10 mM. The effect of each compound on the PTP1B-catalyzed *p*NPP hydrolysis was determined at 25 °C and pH 7.0 in a 200 μl reaction system in a 96-well plate. Each reaction contained 10 μl of 2 mM compound in DMSO (final concentration 100 μM) and 190 μl assay buffer (50 mM 3,3-dimethylglutarate, 1 mM EDTA, 1 mM DTT, pH 7.0 with an ionic strength of 0.15 M adjusted by addition of NaCl) containing 2 mM *p*NPP and 10 nM PTP1B. The PTP-catalyzed reaction was started by addition of the PTP1B. Ten μl of DMSO (i.e. no aryl diketoacid) was used as a control. The PTP1B-catalyzed hydrolysis of *p*NPP was measured by monitoring the absorbance at 405 nm of the product *p*-nitrophenol continuously, with a SpectraMAX Plus 384 microplate spectrophotometer (Molecular Devices). The initial rate was obtained by calculating the slope of the product versus the time curve. The IC_{50} value was determined by plotting relative PTP activity toward *p*NPP activity versus inhibitor concentration and fitting to equation [1] using SigmaPlot 10.0.

$$V_i/V_0 = IC_{50}/(IC_{50} + [I]) \quad [1]$$

In this case, V_i is the reaction velocity when the inhibitor concentration is [I], V_0 is the reaction velocity with no inhibitor, and $IC_{50} = K_i + K_i[S]/K_m$.

K_i Measurement

The PTP1B-catalyzed hydrolysis of *p*NPP in the presence of aryl diketoacid was assayed at 25 °C and in the assay buffer described above. The reaction was initiated by addition of PTP1B to a reaction mixture (200 μl) containing various concentrations of *p*NPP (ranging from 0.2 to 5 K_m) and various fixed concentrations of aryl diketoacid, and quenched by addition of 50 μl of 5 M NaOH. Nonenzymatic hydrolysis of the substrate was corrected by measuring the control without addition of enzyme. The amount of product *p*-nitrophenol was determined from the absorbance at 405 nm detected by a SpectraMAX Plus 384 microplate spectrophotometer using a molar extinction coefficient of 18,000 $M^{-1}cm^{-1}$. The inhibition constant and inhibition pattern were evaluated using the program SigmaPlot 10.0.

Crystallization of PTP1B with LZP6 and LZP25 and X-ray Data Collection

All crystallization experiments were carried out at 4 °C using the hanging drop vapor diffusion methods. For co-crystallization, 20 μl of PTP1B stock (~7.0 mg/ml) in 100 mM MES (pH 6.5), 50 mM NaCl, 0.1 mM EDTA, and 3.0 mM DTT was mixed with 1 μl of LZP6 or LZP25 stock solutions (20 mM in DMSO). Crystals of PTP1B•LZP25 and PTP1B•LZP6 were obtained at 4 °C by vapor diffusion in hanging drops. The protein drops were equilibrated against a reservoir solution containing 20% w/v polyethylene glycol 3350, 200 mM magnesium acetate tetrahydrate, and 100 mM HEPES buffer (pH 7.7). The crystals of PTP1B•LZP6 and PTP1B•LZP25 both belonged to space group $P3_121$ (Table 3)

For X-ray data collection, the crystals were transferred into 5 μl of cryoprotectant buffer containing 30% w/v polyethylene glycol 3350, 100 mM NaCl, and 100 mM HEPES (pH 7.7), and were allowed to soak for 30 minutes. The crystals were then flash-cooled by liquid nitrogen. X-ray data were collected at 100 K on a Rigaku RU-300 rotating anode generator (Rigaku/MSC) equipped with focusing mirrors (MSC/Yale) and an R-AXIS IV++ image plate detector. Data were processed using the program HKL,[20] and the statistics are provided in Table 3.

Structural Determination and Refinement

The structure of PTP1B•LZP25 was solved by molecular replacement using the program AmoRe.[21] The structure of PTP1B (PDB entry code 1pxh),[22] without the solvent molecules and the bidentate inhibitor, was used as a search model. The resulting difference Fourier map indicated some alternative tracing, which was incorporated into the model. The map revealed the density for the bound LZP25 in the active site of PTP1B. The structure was refined to 2.4 Å resolution with the program CNS,[23] first using simulated annealing at 3,000 K, and then alternating positional and individual temperature factor refinement cycles. The progress of the refinement was evaluated by the improvement in the quality of the electron density maps, and the reduced values of the conventional *R* factor ($R = |\Sigma_h||Fo|-|Fc||/\Sigma_h|Fo|$), and the free *R* factor (3.5 % of the reflections omitted from the refinement).[24] Electron density maps were inspected and the model was modified on an interactive graphics workstation with the program O.[25] Finally, water molecules were added gradually as the refinement progressed. They were assigned in the $|Fo|-|Fc|$ difference Fourier maps with a 3δ cutoff level for inclusion in the model.

The structure of PTP1B•LZP6 was solved by molecular replacement using the structure of PTP1B•LZP25 as the search model (except that LZP25 and solvent molecules were omitted). The map revealed very good density for the bound LZP6 in the active site of PTP1B. The structure was refined at 1.9 Å with the program CNS (Table 3), following a protocol similar to that described above.

Cell Lines and Tissue Culture

Human hepatoma cells (HepG2) were obtained from ATCC (HB-8065). HepG2 cells were grown and maintained in Minimum essential Medium (MEM, Eagle) with 2 mM L-glutamine, 1 mM sodium pyruvate and 10% fetal bovine serum in a 5% CO_2 environment.

Immunoblotting

Sixty to eighty percent confluent HepG2 cells were starved for 5 hours in MEM without serum. Next, cells were treated for 20 min with a range of concentrations of LZP25 or LZP6, followed by stimulation with or without 100 nM insulin for 5 min. Incubation was terminated by removing the fluid and cells were washed with cold PBS. Cells were scraped and lysed with lysis buffer (50 mM Tris-HCl, pH 7.5, 150 mM NaCl, 1% NP-40, 10 mM sodium phosphate, 10 mM NaF, 1 mM EDTA, 2 mM orthovanadate, 5 mM iodoacetic acid, 5 mg/ml leupeptin, 5 mg/ml aprotinin, 0.1 mg/ml PMSF, and 1 mM benzamidine). After 30 min lysing on ice, the cell lysate was centrifuged at 13,200 rpm for 15 min. Total cellular proteins were separated by SDS-PAGE and transferred electrophoretically to a nitrocellulose membrane, which was immunoblotted by anti-phospho-IRβ antibodies. To confirm the equal sample loading, the membrane was also probed with anti-β-actin antibody. Blots were developed using a western blot detection kit (upstate) according to the manufacturer's instructions. Western blotting images were analyzed with Image J (NIH).

Results and Discussion

Aryl Diketoacid Derivatives as PTP1B Inhibitors

One of the most efficient methods for the acquisition of active site-directed, reversible, potent and selective PTP1B inhibitors is to tether a nonhydrolyzable pTyr mimetic to an appropriately functionalized chemical moiety, which makes it possible to target both the active site and a unique nearby sub-pocket.[14] Although numerous pTyr surrogates have been reported,[26] they are generally not drug-like, and usually have limited cell membrane permeability. Thus, there is continued interest in developing novel pTyr mimetics with more acceptable pharmacological properties.[27] The aryl diketoacid scaffold has been used successfully for the design of HIV-1 integrase inhibitors.[28] Given the structural similarity between aryl diketoacids and pTyr, we were intrigued to find out whether aryl diketoacids possess any inhibitory activity against PTP1B. A number of aryl diketoacid derivatives were synthesized (Figure 1, and Materials & Methods). The ability of these compounds to inhibit PTP1B-catalyzed hydrolysis of *p*-nitrophenyl phosphate (*p*NPP) was assessed at pH 7 and 25 °C (for details see Experimental Section). As shown in Table 1, simple aryl diketoacids (LZP36, LZP3, and LZP39) exhibit no inhibitory activity at 100 μM against PTP1B, while substitutions at the para- or meta- position of the phenyl ring with benzyl moieties bring the IC_{50} values of compounds LZP4, LZP38 and LZP25 to the low micromolar range. Clearly, bulky hydrophobic substitutions on the phenyl ring enhance the affinity of aryl diketoacids for PTP1B. We then determined whether dimerization of the aryl diketoacids would improve inhibition of PTP1B activity. Aryl diketoacid dimer formation was achieved through either a piperazino or cyclohexane-1,4-*trans*-diamine linker (Figure 1). To our delight, the piperazine- or cyclohexane diamine-linked aryl diketoacid dimers LZP6, LZP7, LZP37, and LZP40 showed improved PTP1B inhibitory activity over the corresponding monomers (LZP4, LZP25, and LZP38), with IC_{50} values in the low micromolar range (Table 2).

To determine the inhibition constant and mode of inhibition by LZP25 and LZP6, the effect of the inhibitors on PTP1B-catalyzed reaction was studied at 8 different *p*NPP and 4 different compound concentrations. As shown by the Lineweaver-Burk plot in Figure 2, PTP1B-catalyzed *p*NPP hydrolysis in the presence of LZP25 displayed the characteristic intersecting line pattern for noncompetitive inhibition, with a K_i value 16.3 ± 1.1 μM. The observation that

LZP25, a putative pTyr surrogate, was not competitive with substrate is rather intriguing. This is especially so because noncompetitive PTP1B inhibitors have previously been found to bind an allosteric site located ~20 Å from the active site.[29] Kinetic analysis indicated that dimeric LZP6 is also a noncompetitive inhibitor of PTP1B with a K_i of 12 ± 0.6 μM. Noncompetitive inhibition of PTP1B-catalyzed reaction by LZP25 and LZP6 was also apparent when the data were analyzed by Eadie-Hofstee plot (Figure S1). Given the lack of a formal charge in the aryl diketoacid dimer, it is not at all clear where the binding site for LZP6 is in PTP1B. To provide insight into the molecular basis for PTP1B inhibition by LZP25 and LZP6, we decided to solve the three-dimensional structure of the complexes.

Structures of the PTP1B•LZP25 Complex

Using conditions similar to those described previously,[19,22] we produced crystals of the PTP1B•LZP25 complex that diffracted to 2.4 Å resolution (Table 3). The structures were solved by molecular replacement. The final model for the PTP1B•LZP25 complex included PTP1B residues 2-284 and all atoms of the inhibitor. Binding of pTyr or nonhydrolyzable pTyr mimetics are usually accompanied by the closure of the flexible WPD loop (residues 179-187).[19,22,30] Thus it was striking to find that the WPD loop adopts an open conformation; the overall structure of PTP1B•LZP25 is similar to the ligand-free PTP1B structure in the WPD loop open form,[31] with root-mean-square derivation (RMSD) for all α-carbon positions between the two being 0.499 Å. The major difference between the two structures is electron density in the PTP1B active site corresponding to LZP25, which was confirmed by analyzing the $2F_o$ - F_c and F_o - F_c difference Fourier maps with contour levels of 1.0 and 2.5 δ, respectively (Figure 3A).

As shown in Figure 3B, LZP25 occupies the PTP1B active-site pocket whose base corresponds to the phosphate-binding loop or P-loop (residues 214-221). The diketoacid moiety makes two hydrogen bonds with the main chain amides of the P-loop, one polar interaction with the side chain of Arg221, one hydrogen bond with the hydroxyl side chain of Ser216, and two additional polar interactions with the side chains of Gln266 and Tyr46, respectively. Besides these polar interactions, there are also ample van der Walls contacts between PTP1B and LZP25. For example, the phenyl ring immediately attached to the diketoacid has extensive hydrophobic interactions with the side chains of residues lining up the active site cavity, including Tyr46, Val49, Ala217 and Ile219. There are also van der Walls contacts between the two carbon atoms of the terminal ketoacid moiety and the side-chain of Gln262. Additionally, one of the distal phenyl rings in LZP25 forms hydrophobic interactions with residues Asp48 and Gln262, while the other makes van der Walls contacts with residues Tyr46, Arg47, and Asp48. These additional non-polar interactions with the distal phenyl ring(s) may be responsible for the higher affinity of LZP4, LZP38, and LZP25, in comparison with those (LZP36, LZP3, and LZP39) that lack the distal aromatic substitutions (Table 1).

Why Is the WPD Loop in the Open Conformation in the PTP1B•LZP25 Complex?

Enzymes require conformational flexibility to control solvent accessibility, recruit functional residues for catalysis, and/or facilitate the binding and release of substrate or product. For the PTPs, the major conformational change essential to substrate binding and catalysis is restricted to the movement of the WPD loop, which harbors the general acid/base (Asp181 in PTP1B). Crystallographic studies have captured the WPD loop either in the open or closed conformations.[30,32,33] Spectroscopic measurements indicate that in solution ligand-free PTP exists as an equilibrium mixture of both the open and closed froms, and that ligand binding stabilizes the closed conformation.[34-36]

Although LZP25 occupies the active site, the manner by which it interacts with PTP1B is significantly different from those observed between pTyr and PTP1B (Figure 3C). A key

difference is how Arg221 in the P-loop is engaged by the ligand. When pTyr or an optimal nonhydrolyzable pTyr mimetic is bound at the active site, a bidentate hydrogen bond is formed between the oxyanion and the guanidinium group of Arg221.[19,22,30] This event triggers a series of interactions between Arg221 and the side chains of the invariant Glu115 as well as Trp179 in the WPD loop, which are likely responsible for the stabilization of the closed conformation.[37-39] The phenyl ring of pTyr is then effectively buried within the active site cavity, created by the nonpolar side-chains of Ala217 and Ile219 of the P-loop, Phe182 of the WPD loop, Tyr46, Val49 and Gln262. In stark contrast, the interactions between the diketoacid moiety of LZP25 and the P-loop including Arg221 are less optimal and insufficient to trigger the WPD loop closure. Moreover, the position of the diketoacid proximal phenyl ring is nearly perpendicular to that of pTyr, which would cause a steric clash with Phe182 if the WPD loop were in the closed conformation. Thus the WPD loop adopts an open conformation in the PTP1B•LZP25 complex. It appears that depending on the specific interactions with the PTP, an active site-directed ligand can either bind the active site cleft in the WPD loop open or closed conformation.

Structure of the PTP1B•LZP6 Complex

Dimerization of aryl diketoacids through a piperazino or cyclohexane-1,4-*trans*-diamine linkage generated several PTP1B inhibitors with improved potencies over their monomeric counterparts (Tables 1 & 2). This is a novel finding because, unlike other PTP1B inhibitors, these dimeric compounds have no negative charge(s), which are usually required for binding to the highly positively charged PTP active site. To better understand the mode of interaction between PTP1B and the aryl diketoacid dimers, we determined the crystal structure of PTP1B in complex with LZP6, which was refined to 1.9 Å resolution (Table 3). The final model for PTP1B•LZP6 includes residues 2-283 and all atoms of LZP6. The overall structure of PTP1B in the complex is similar to that of PTP1B•LZP25, with RMSD between all α-carbon positions of the two structures at 0.211 Å. Similar to LZP25, LZP6 was unambiguously identified by well-defined electron densities in the active site, and the WPD loop in the PTP1B•LZP6 structure is also in the open conformation (Figure 4A). However, the mode of LZP6 binding is completely different from that of LZP25. Only one of the aryl diketoacid (monomer A), including the piperazino linker, is actively engaged with the PTP1B active site, while the other half (monomer B) of LZP6 appears to be solvent exposed (Figure 4B). Unlike LZP25, which has numerous polar interactions with PTP1B, only one electrostatic contact is evident between Lys118 and O_{B3} of LZP6, which is mediated by a water molecule. Instead, binding between PTP1B and LZP6 is dominated by hydrophobic interactions (Figure 4B). Specifically, the phenyl ring directly adjacent to the keto group in monomer A makes numerous van der Waals contacts with the side chains of Tyr46, Ser216, Ala217, Ile219, and Gln262. Interestingly, this phenyl ring sits at approximately the same location occupied by the aromatic moiety of pTyr seen in the PTP1B•pTyr complex (Figure 4C and ref.[19]). In addition, the piperazine linker also makes hydrophobic contacts with Tyr46. Without any formal charge, the terminal phenyl ring in monomer A does not point to the bottom of the active site and interact with the P-loop, as is the case for the phosphoryl group in pTyr. Rather, the ring extends across the active site cleft and makes multiple non-polar interactions with the side chains of Trp179, Phe182, Arg221, and Thr263 (Figure 4B). Specific interactions between LZP6 terminal phenyl ring and residues Trp179 and Phe182 also effectively block the WPD loop closure, thereby providing a structural basis for the open conformation observed in the PTP1B•LZP6 complex. Collectively, the structure reveals that LZP6 binds PTP1B in the WPD loop open conformation and covers the active site pocket like a lid.

Although half of the LZP6 molecule appears to be exposed in the solvent, symmetry operation suggests that the two phenyl rings in monomer B may interact with the side chains of Phe196 and Phe280 from another PTP1B molecule in the crystal (Figure 4D). This observation is

interesting because residues Phe196 and Phe280 have been previously shown to define a hydrophobic pocket, located ~20 Å from the active site, that was occupied by an allosteric inhibitor of PTP1B.[29] To ascertain the significance of these symmetry related interactions, we replaced either Phe196 or Phe280 with an Ala and evaluated the effect on LZP6 binding affinity. As shown in Table 4, IC_{50} values of LZP6 for F196A and F280A were not significantly different from that of the wild-type enzyme, suggesting that LZP6 is unlikely to interact with these residues in solution. Similarly, Arg47 does not participate in LZP6 binding and the Arg47 to Val substitution does not alter the IC_{50} value for LZP6. On the contrary, substitutions at Phe182, Gln262, and Thr263 reduced PTP1B's affinity for LZP6 by 3-4 fold, which is consistent with the structural observations that these residues contribute to binding LZP6 (Figure 4C). Overall mutational data support the conclusion that symmetry related interactions between LZP6 monomer B and Phe196 and Phe280 are likely the result of crystal packing.

To further substantiate the observed binding mode between PTP1B and LZP6, we analyzed several compounds structurally related to LZP6 (Table 2). LZP7, LZP37, and LZP40 possess chemical entities similar to those present in LZP6 that are known to be important for interactions with PTP1B active site. Accordingly, these compounds possess either comparable (LZP7) or enhanced (LZP37 and LZP40) inhibitory activities to that of LZP6. In contrast, LZP8 and LZP9 lack the terminal phenyl ring predicted to make a number of key contacts with PTP1B. As expected, they are less potent than LZP6 and exhibit no inhibitory activity against PTP1B at 100 μM. To directly test whether one aryl diketoacid moiety is sufficient for binding, we synthesized monomeric versions of LZP6 and LZP40, in which one of the aryl diketoacid is replaced by a *tert*-butyl dicarbonate (BOC) group. As shown in Table 2, the IC_{50} values of LZP70 and LZP71 are slightly higher (2-3 fold) than those of LZP6 and LZP40, supporting the conclusion that LZP6 is involved in a novel mode of interaction with PTP1B active site and only half of the aryl diketoacid dimer is required for binding.

Structural and Mechanistic Basis for Noncompetitive PTP1B Inhibition by LZP25 and LZP6

Two major mechanisms of reversible enzyme inhibition are commonly described in textbooks. In competitive inhibition, the inhibitor binds to the active site in place of the substrate, thus preventing the enzyme-catalyzed reaction. Competitive inhibition increases the apparent K_m, which can be overcome by high substrate concentration due to mass action. In noncompetitive inhibition, the inhibitor binds to the enzyme at an allosteric site that is distinct from the active site. This type of inhibition reduces the maximum rate of an enzymatic reaction without affecting the apparent binding affinity of the enzyme for the substrate. The decrease in V_{max} occurs as a result of conformational changes in the active site induced by the presence of the inhibitor in the allosteric site.

Our kinetic analyses indicate that LZP25 and LZP6 act as noncompetitive inhibitors of PTP1B. Unlike classical noncompetitive inhibitors, however, both LZP25 and LZP6 occupy the active site, rather than an allosteric site away from the active site. Although the specific binding modes differ between the two compounds, one common feature from the structures of PTP1B•LZP25 and PTP1B•LZP6 is that the WPD loop is in the open conformation. Molecular modeling suggests that substrate *p*NPP can still be accommodated by PTP1B's active site in the presence of either LZP25 or LZP6 (Figure 5). Because PTP catalysis requires the WPD loop in the closed conformation, which positions the general acid Asp181 close to the scissile oxygen of the substrate for efficient proton transfer,[37-39] the LZP25- or LZP6-bound PTP1B is catalytically incompetent. Consequently, substrate turnover cannot occur when LZP25 or LZP6 is present in the PTP1B active site, because the catalytically essential residues are not optimally aligned to promote *p*NPP hydrolysis. Thus, consistent with the mode of noncompetitive inhibition, there is no competition between the aryl diketoacid-based inhibitors and the substrate. The mechanism for LZP25 and LZP6-mediated PTP1B inhibition derives from the fact that they

stabilize the open, inactive conformation of the WPD loop, thereby reducing the concentration of the catalytically competent enzyme, leading to a decrease in V_{max}.

Cellular Activity of LZP25 and LZP6

Given the observed potency of LZP25 and LZP6 for PTP1B, we proceeded to evaluate their ability to inhibit PTP1B inside the cell. Previous studies have demonstrated that PTP1B serves as a negative regulator of the insulin activated signaling pathways by catalyzing the dephosphorylation of the insulin receptor β (IRβ) subunit. Thus, inhibition of PTP1B activity should enhance insulin signaling. Indeed, IRβ phosphorylation in the liver of the PTP1B knockout mice is prolonged by 2-fold.[3,4] PTP1B knockdown by antisense in rat hepatoma cells yields a 2.3-fold increase in the level of phosphorylated IRβ.[40] In addition, significant enhancements in IRβ phosphotyrosine levels are also observed with cell permeable analogs of a potent and selective small molecule PTP1B inhibitor.[41]

To examine the specificity of LZP25 and LZP6 for PTP1B, their inhibitory activity toward a panel of PTPs including cytosolic PTPs, HePTP, SHP2, and Lyp, the receptor-like PTPs, LAR and PTPα, and the dual specificity phosphatase VHR, was determined. As shown in Table 5, LZP25 and LZP6 display at least several fold selectivity for PTP1B over all PTPs examined.

To determine the cellular efficacy of LZP25 and LZP6, we assessed their effect on insulin signaling in human hepatoma HepG2 cells. The cells were incubated with either 150 μM (7.5 of the IC_{50} value) LZP25 or 60 μM (3.75x of the IC_{50} value) LZP6 for 20 minutes and subsequently treated either with or without insulin (100 nM) for 5 min. Cell lysates were resolved by SDS-PAGE, then the proteins were transferred to nitrocellulose membranes and probed with anti-phospho-IRβ (pY1162/pY1163) antibodies. As shown in Figure 6A, incubation of cells with LZP25 had no significant effect on IRβ phosphorylation, while LZP6 treatment increased insulin stimulated IRβ phosphorylation by 230%. Given that LZP25 and LZP6 have similar affinity for PTP1B, the results suggest that LZP25 is not cell permeable whereas LZP6 is capable of penetrating the cellular membrane. If the carboxylic acid in LZP25 obstructs cell membrane penetration, then masking the acid with the piperazino linker should improve its cellular activity. Indeed, when cells were treated with LZP70 or LZP71 at ~4x of their respective IC_{50} values, both compounds were able to augment the insulin stimulated IRβ phosphorylation to the same extent (~2-fold) as effected by LZP6 at equivalent concentration (Figure 6B). We further demonstrated that LZP6 can potentiate insulin signaling in a dose dependent manner, exhibiting cellular activity at both 15 and 30 μM (1 and 2× IC_{50}) concentrations (Figure 6C).

Implications for PTP1B Inhibitor Development

As mentioned above, there is compelling evidence that define PTP1B as an outstanding target for the treatment of a number of human diseases. A major challenge in drug discovery programs targeted toward the PTPs is to identify inhibitory compounds with pharmacologically acceptable bioavailability. Most PTP active site-directed pharmacophores identified at present are negatively charged pTyr mimetics and therefore cannot readily enter the cell. This lack of cell permeability limits the utility of such compounds in signaling studies and further therapeutic development. We show in this study that LZP25 and LZP6 function as noncompetitive PTP1B inhibitors and bind the active site in distinct fashions that effectively block the WPD loop closure, thereby preventing formation of the catalytically competent form of the enzyme. This is in stark contrast to other pTyr mimetics, which bind the WPD loop closed conformation. As depicted in Figure 7, the electrostatic potential and topology of the catalytic cleft are considerably different between the WPD loop open and closed forms. Moreover, with the WPD loop in the open conformation the active site pocket is substantially larger with greater hydrophobic binding surface. Thus in comparison to the WPD closed form,

the open conformation presents a unique opportunity for developing active site-directed PTP inhibitors with improved pharmacological properties.

It has proven difficult to develop effective uncharged PTP active site-directed small molecule inhibitors, due primarily to the electrostatic properties of the PTP active site. We provide the first example in which a neutral compound LZP6 can engage PTP1B active site in such a way as to maintain the open, inactive conformation of the WPD loop, without resorting to electrostatic interactions with the P-loop. Notably, LZP6 exhibits excellent cell permeability and enhances insulin signaling in HepG2 cells. Further increase in potency could be achieved by appending an appropriate chemical group to LZP6 to fill the space taken by *p*NPP (Figure 5B). Moreover, binding specificity can be improved by tethering LZP6 to appropriate functional groups in order to engage additional unique surface areas that border the PTP1B active site. Given the conserved structural and catalytic properties of the PTP active site, it is expected that targeting the inactive, WPD loop open conformation could represent a general and effective strategy applicable to all PTPs.

Supplementary Material

Refer to Web version on PubMed Central for supplementary material.

Acknowledgement

This work was supported by National Institutes of Health Grant CA126937. The work in Y.-Q. Long's lab was in part supported by National Natural Science Foundation of China (30721005).

References

(1). Tonks NK. Nat. Rev. Mol. Cell Biol 2006;7:833–846. [PubMed: 17057753]

(2). Zhang Z-Y. Curr. Opin. Chem. Biol 2001;5:416–423. [PubMed: 11470605]

(3). Elchelby M, Payette P, Michaliszyn E, Cromlish W, Collins S, Loy AL, Normandin D, Cheng A, Himms-Hagen J, Chan CC, Ramachandran C, Gresser MJ, Tremblay ML, Kennedy BP. Science 1999;283:1544–1548. [PubMed: 10066179]

(4). Klaman LD, Boss O, Peroni OD, Kim JK, Martino JL, Zabolotny JM, Moghal N, Lubkin M, Kim YB, Sharpe AH, Stricker-Krongrad A, Shulman GI, Neel BG, Kahn BB. Mol. Cell. Biol 2000;20:5479–5489. [PubMed: 10891488]

(5). Zinker BA, Rondinone CM, Trevillyan JM, Gum RJ, Clampit JE, Waring JF, Xie N, Wilcox D, Jacobson P, Frost L, Kroeger PE, Reilly RM, Koterski S, Opgenorth TJ, Ulrich RG, Crosby S, Butler M, Murray SF, McKay RA, Bhanot S, Monia BP, Jirousek MR. Proc. Natl. Acad. Sci. USA 2002;99:11357–11362. [PubMed: 12169659]

(6). Bjorge JD, Pang A, Fujita DJ. J. Biol. Chem 2000;275:41439–41446. [PubMed: 11007774]

(7). Cheng A, Bal GS, Kennedy BP, Tremblay ML. J. Biol. Chem 2001;276:25848–25855. [PubMed: 11346638]

(8). Liang F, Lee S-Y, Liang J, Lawrence DS, Zhang Z-Y. J. Biol. Chem 2005;280:24857–24863. [PubMed: 15866871]

(9). Dube N, Cheng A, Tremblay ML. Proc. Natl. Acad. Sci. USA 2004;101:1834–1839. [PubMed: 14766979]

(10). Zhai YF, Beittenmiller H, Wang B, Gould MN, Oakley C, Esselman WJ, Welsch CW. Cancer Res 1993;53:2272–2278. [PubMed: 8097963]

(11). Wiener JR, Kerns BJ, Harvey EL, Conaway MR, Iglehart JD, Berchuck A, Bast RC Jr. J. Natl. Cancer Inst 1994;86:372–378. [PubMed: 7905928]

(12). Julien SG, Dubé N, Read M, Penney J, Paquet M, Han Y, Kennedy BP, Muller WJ, Tremblay ML. Nat. Genet 2007;39:338–346. [PubMed: 17259984]

(13). Bentires-Alj M, Neel BG. Cancer Res 2007;67:2420–2424. [PubMed: 17347513]

(14). Zhang S, Zhang Z-Y. Drug Discovery Today 2007;12:373–381. [PubMed: 17467573]

(15). Jiang X-H, Song L-D, Long Y-Q. J. Org. Chem 2003;68:7555–7558. [PubMed: 12968921]

(16). Jiang X-H, Long Y-Q. Chinese J. Chem 2004;22:978–983.

(17). Long Y-Q, Jiang X-H, Dayam R, Sanchez T, Shoemaker R, Sei S, Neamati N. J. Med. Chem 2004;47:2561–2573. [PubMed: 15115398]

(18). Zeng L-F, Jiang X-H, Sanchez T, Zhang H-S, Dayam R, Neamati N, Long Y-Q. Bioorg. Med. Chem 2008;16:7777–7787. [PubMed: 18644730]

(19). Puius YA, Zhao Y, Sullivan M, Lawrence DS, Almo SC, Zhang Z-Y. Proc. Natl. Acad. Sci. USA 1997;94:13420–13425. [PubMed: 9391040]

(20). Otwinowski Z, Minow W. Methods Enzymol 1997;276:307–326.

(21). Navaza J. Acta Cryst 1994;A50:157–163.

(22). Sun J-P, Fedorov AA, Lee S-Y, Guo X-L, Shen K, Lawrence DS, Almo SC, Zhang Z-Y. J. Biol. Chem 2003;278:12406–12414. [PubMed: 12547827]

(23). Brünger AT, Adams PD, Clore GM, DeLano WL, Gros P, Grosse-Kunstleve RW, Jiang JS, Kuszewski J, Nilges M, Pannu NS, Read RJ, Rice LM, Simonson T, Warren GL. Acta Crystallogr., Sect. D: Biol. Crystallogr 1998;54:905–921. [PubMed: 9757107]

(24). Brünger AT. Nature 1992;355:472–475. [PubMed: 18481394]

(25). Jones TA, Zou JY, Cowan SW, Kjeldgaard GJ. Acta Crystallogr. Sect. A 1991;47:110–119. [PubMed: 2025413]

(26). ZhangZ-YBradshawRalphDennisEdward, Editors-in-Chief, Handbook of Cell Signaling20031677684Academic Press

(27). Combs AP, Yue EW, Bower M, Ala PJ, Wayland B, Douty B, Takvorian A, Polam P, Wasserman Z, Zhu W, Crawley ML, Pruitt J, Sparks R, Glass B, Modi D, McLaughlin E, Bostrom L, Li M, Galya L, Blom K, Hillman M, Gonneville L, Reid BG, Wei M, Becker-Pasha M, Klabe R, Huber R, Li Y, Hollis G, Burn TC, Wynn R, Liu P, Metcalf B. J. Med. Chem 2005;48:6544–6548. [PubMed: 16220970]

(28). Pais GC, Burke TR. Drugs of the Future 2002;27:1101–1111.

(29). Wiesmann C, Barr KJ, Kung J, Zhu J, Erlanson DA, Shen W, Fahr BJ, Zhong M, Taylor L, Randal M, McDowell RS, Hansen SK. Nat. Struct. Mol. Biol 2004;11:730–737. [PubMed: 15258570]

(30). Jia Z, Barford D, Flint AJ, Tonks NK. Science 1995;268:1754–1758. [PubMed: 7540771]

(31). Barford D, Flint AJ, Tonks NK. Science 1994;263:1397–404. [PubMed: 8128219]

(32). Stuckey JA, Schubert HL, Fauman E, Zhang Z-Y, Dixon JE, Saper MA. Nature 1994;370:571–575. [PubMed: 8052312]

(33). Schubert HL, Fauman EB, Stuckey JA, Dixon JE, Saper MA. Protein Sci 1995;4:1904–1913. [PubMed: 8528087]

(34). Juszczak LJ, Zhang Z-Y, Wu L, Gottfried DS, Eads DD. Biochemistry 1997;36:2227–2236. [PubMed: 9047324]

(35). Wang F, Li W, Emmett MR, Hendrickson CL, Marshall AG, Zhang Y-L, Wu L, Zhang Z-Y. Biochemistry 1998;37:15289–15299. [PubMed: 9799489]

(36). Khajehpour M, Wu L, Liu S, Zhadin N, Zhang Z-Y, Callender R. Biochemistry 2007;46:4370–4378. [PubMed: 17352459]

(37). Keng Y-F, Wu L, Zhang Z-Y. Eur. J. Biochem 1999;259:809–814. [PubMed: 10092868]

(38). Hoff RH, Hengge AC, Wu L, Keng Y-F, Zhang Z-Y. Biochemistry 2000;39:46–54. [PubMed: 10625478]

(39). Zhang Z-Y. Progress in Nucleic Acid Research and Molecular Biology 2003;73:171–220. [PubMed: 12882518]

(40). Clampit JE, Meuth JL, Smith HT, Reilly RM, Jirousek MR, Trevillyan JM, Rondinone CM. Biochem Biophys Res Commun 2003;300:261–267. [PubMed: 12504077]

(41). Xie L, Lee SY, Andersen JN, Waters S, Shen K, Guo XL, Moller NP, Olefsky JM, Lawrence DS, Zhang ZY. Biochemistry 2003;42:12792–804. [PubMed: 14596593]

(42). Nicholls A, Sharp KA, Honig B. Proteins, Structure, Function and Genetics 1991;11:281–296.

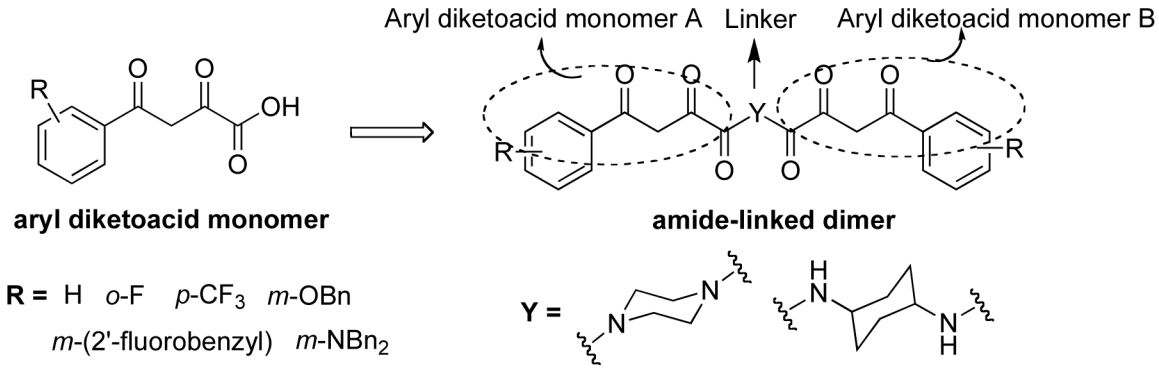

Figure 1.
Structures of the aryl diketoacid derivatives.

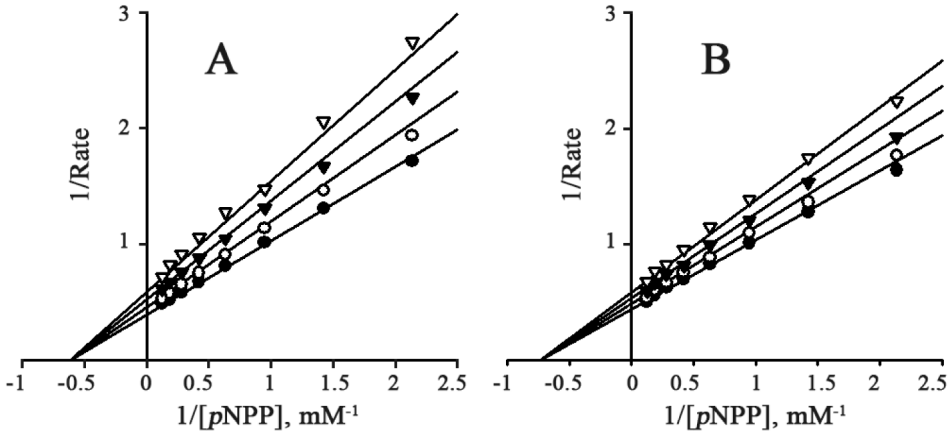

Figure 2.

The effect of LZP25 (A) and LZP6 (B) on PTP1B-catalyzed *p*NPP hydrolysis. The Lineweaver-Burk plot displayed the characteristic intersecting line pattern, consistent with noncompetitive inhibition. The experiment was performed at 25 °C and pH 7.0. (A) LZP25 concentrations were 0 (●), 2.5 (○), 5 (▼), and 7.5 μM (▽), respectively. (B) LZP6 concentrations were 0 (●), 1.25 (○), 2.5 (▼), and 3.75 μM (▽), respectively.

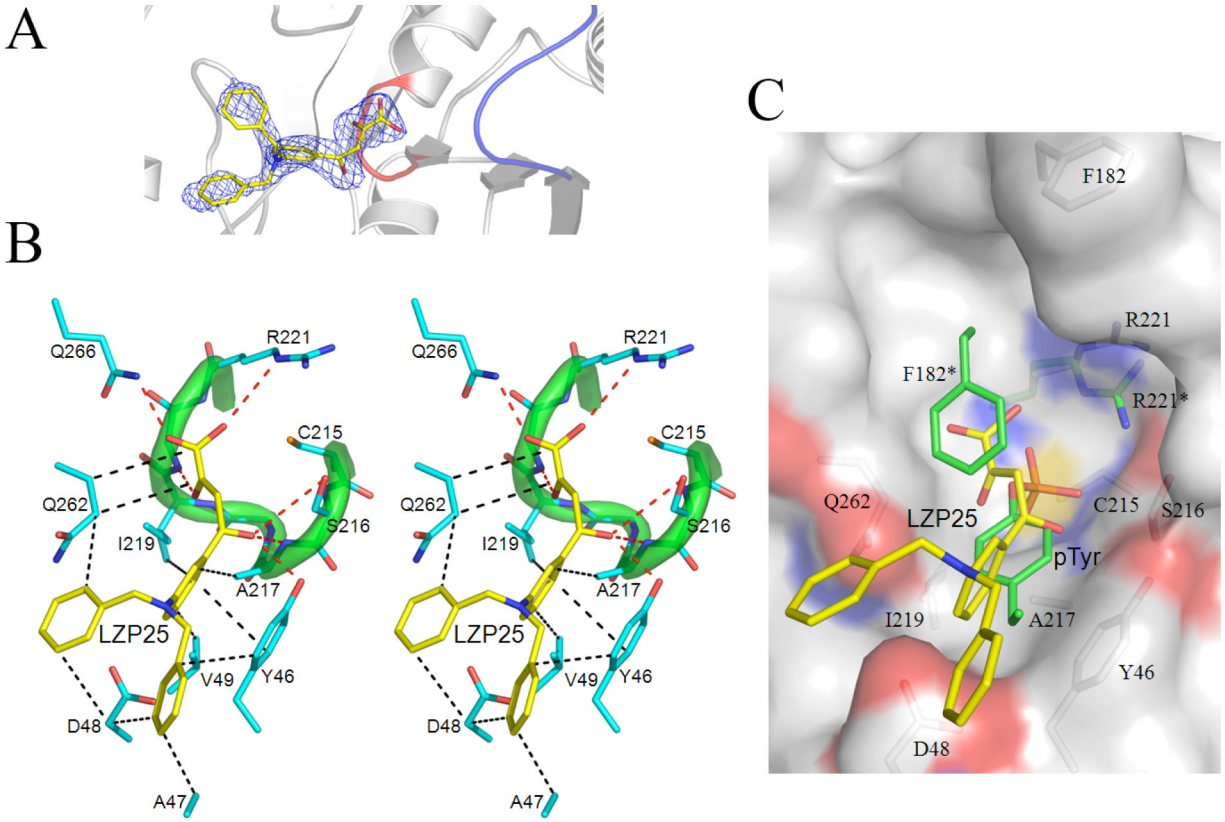

Figure 3.

Crystal structure of PTP1B in complex with LZP25. (A) Electron density map at the active site contoured at 1.0 σ level. The P-loop and WPD loop are shown in red and blue, respectively. (B) Binding mode of LZP25 in the active site of PTP1B. Atomic colors are as follows: oxygen - red, carbon — cyan, sulfur - orange, nitrogen - blue. Ligand's carbon atoms are colored yellow. Key interactions are highlighted with dash lines as follows: electrostatic interactions with the ligand are shown in red, and hydrophobic interactions with ligands are shown in black. P-loop of PTP1B is shown with transparent green cartoon. (C) Superposition of PTP1B•LZP25 and PTP1B•pTyr, the superposition was calculated with active site residues without the ligands. Residues marked with * are in the WPD loop closed conformation. Atomic colors are as follows: oxygen - red, carbon — white, sulfur - orange, nitrogen - blue. LZP25's carbon atoms are colored yellow, while carbon atoms from PTP1B•pY (PDB entry code 1EEN) are colored green.

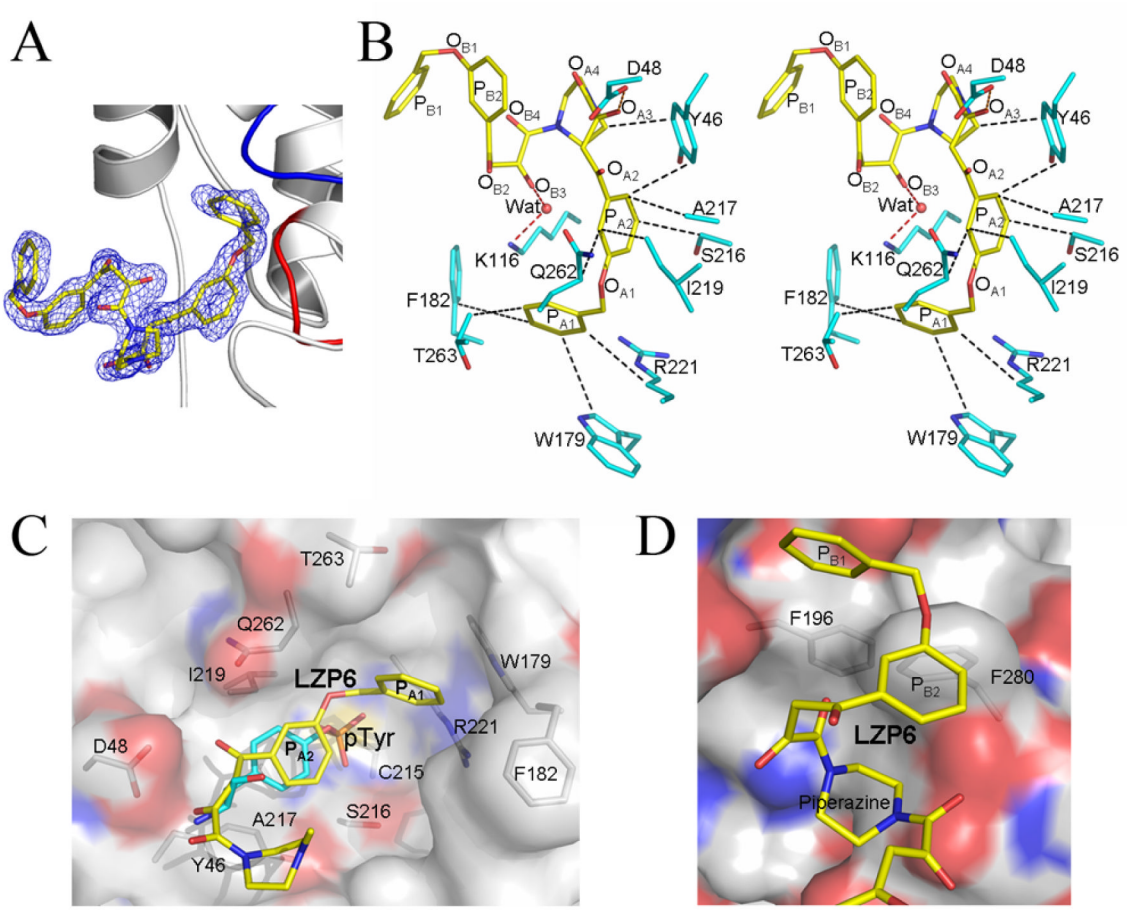

Figure 4.

Crystal structure of PTP1B in complex with LZP6. (A). Electron density map of LZP6 was contoured at 1.2 δ level in blue. Atoms were colored according to atom type (carbon in yellow, oxygen in red, and nitrogen in blue). The P-loop and WPD loop are shown in red and blue, respectively. (B). Binding modes of LZP6 in the active site of PTP1B: Atomic colors are as follows: oxygen - red, carbon — cyan, sulfur - orange, nitrogen - blue. Ligand's carbon atoms are colored yellow. Key interactions are highlighted with dash lines as follows: electrostatic interactions with the ligand are shown in red, and hydrophobic interactions with ligands are shown in black. (C) Superposition of PTP1B•LZP6 and PTP1B•pTyr, the superposition was calculated with active site residues without the ligands. Active site of PTP1B in the open conformation is shown by transparent surface representation, and key residues are shown in stick model. Phenyl rings P_{B1} and P_{B2} of LZP6 are not shown. Atomic colors are as follows: oxygen - red, carbon — white, sulfur - orange, nitrogen - blue. Carbon atoms of LZP6 are colored yellow, and pTyr's carbon atoms are colored green. (D) A symmetry related interaction between LZP6 monomer B and PTP1B. LZP6 is shown as a stick model, PTP1B is shown by transparent surface representation. Color scheme for surface: carbon, white; oxygen, red; nitrigen, blue.

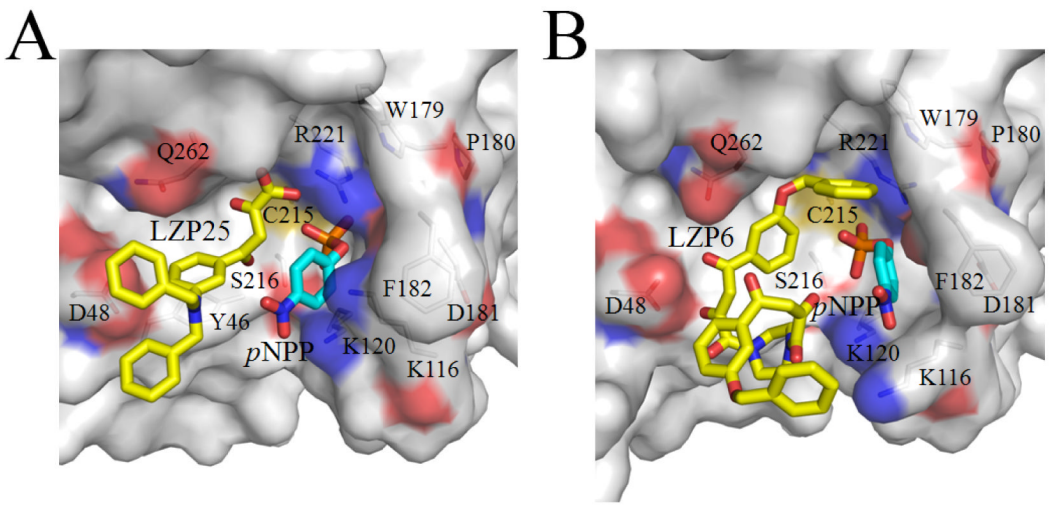

Figure 5.
Modeling of *p*NPP binding to PTP1B in the presence of LZP25 (A) or LZP6 (B). The structures of PTP1B•LZP25 and PTP1B•LZP6 were utilized as the starting points molecular modeling. *p*NPP was manually docked into active site of PTP1B in the presence of LZP25 or LZP6, and energy minimized using program CNS.[23]

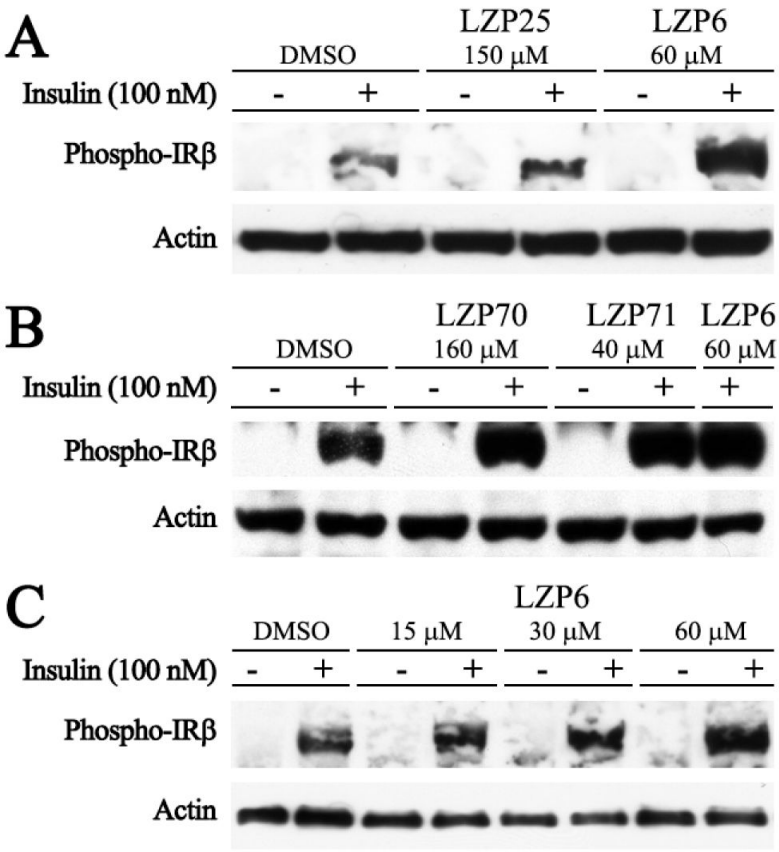

Figure 6.

Cellular activity of aryl diketoacid derivatives. (A) Effect of LZP25 and LZP6 on insulin-mediated IRβ phosphorylation in HepG2 cells. (B) Effect of LZP70 and LZP71 on insulin-mediated IRβ phosphorylation in HepG2 cells. (C) Concentration dependence of LZP6 on insulin-mediated IRβ phosphorylation in HepG2 cells.. Subconfluent HepG2 cells were preincubated with either LZP25 or LZP6 20 min, followed by a 5 min treatment with or without 100 nM insulin. Cell lysates were subjected to SDS-PAGE and the resolved proteins transferred to nitrocellulose membranes, which were probed with anti-phospho-IRβ antibodies. β-actin was used as a loading control.

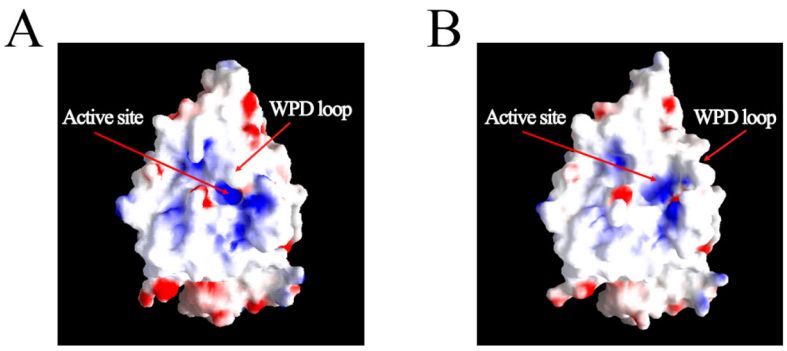

Figure 7.
Surface representations of PTP1B in the WPD loop closed (A) and open (B) conformation. The figure was prepared using GRASP.[42]

Table 1

PTP1B Inhibition by Aryl Diketoacids

Aryl Diketo Acids	Structure	IC_{50}(μM)
LZP36	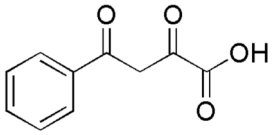	>100
LZP3	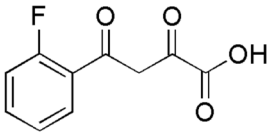	>100
LZP39	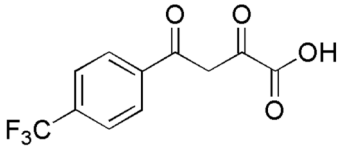	>100
LZP4	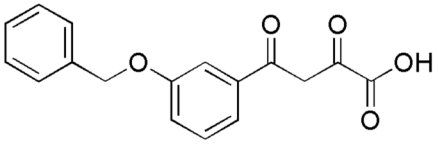	74 ± 16
LZP38	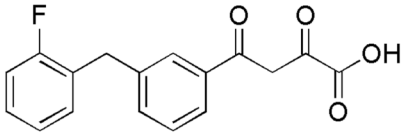	40 ± 8
LZP25	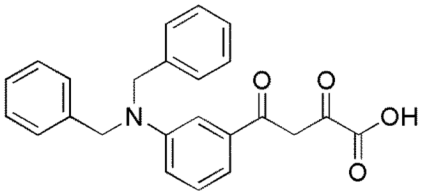	20 ± 5 K_i=16.3± 1.1

Table 2

Inhibition of PTP1B by Amide-linked Aryl Diketoacid Dimers

Aryl Diketoacid Dimers	Structure	IC_{50} (μM)
LZP6	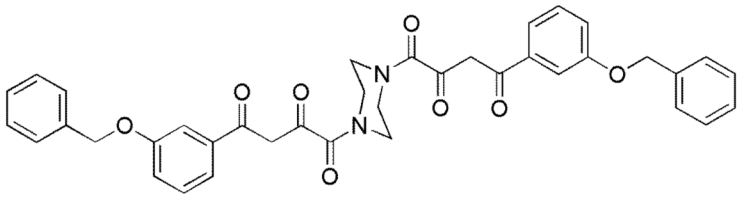	16 ± 2 (K_i=12± 0.6)
LZP7	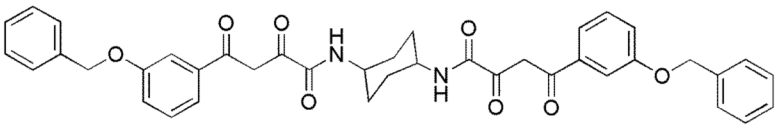	15 ± 3.8
LZP37	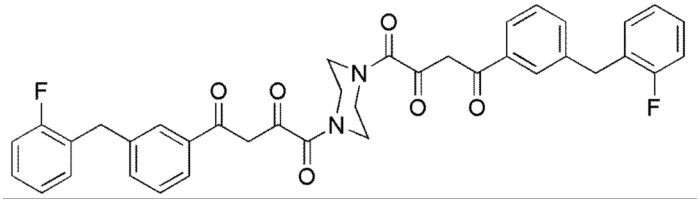	3.7 ± 0.5 (K_i=4.3± 0.7)
LZP40	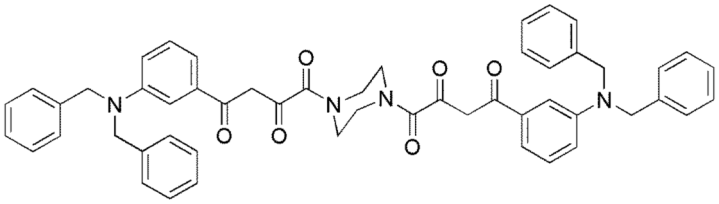	2.8 ± 1.0
LZP8	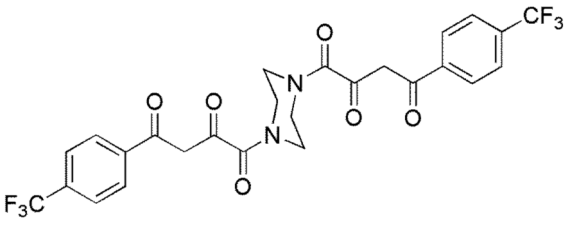	>100
LZP9	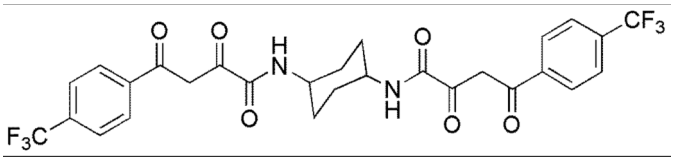	>100
LZP70	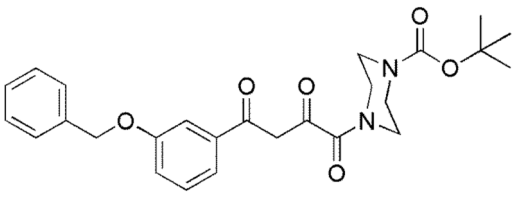	39.5 ± 9

Aryl Diketoacid Dimers	Structure	IC_{50} (μM)
LZP71	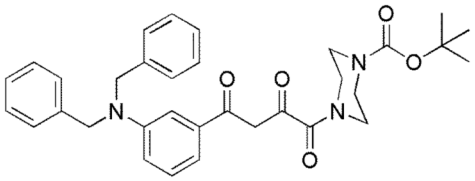	9.2 ± 0.6

Table 3

Crystallographic Data and Refinement Statistics

	PTP1B•LZP25	PTP1B•LZP6
Crystal Parameters		
Space group	$P3_121$	$P3_121$
Cell dimensions (Å)		
a=b	88.5	88.6
c	104.7	104.3
Data Collection		
Resolution (Å)	50-2.4	50-1.6
No. of unique reflections	17,995	54,300
Completeness (%)	94.7	87.4
Redundancy	4.2	3.1
R_{merge} [a]	8.6	12.4
Refinement		
Resolution limit (Å)	50-2.4	50-1.9
No. of Reflections used ($F \geq 2\delta(F)$)	17,214	36,242
No. of protein atoms	2,297	2,297
No. of inhibitor	1	1
No. of water	157	85
R_{work} [b] / $_{Rfree}$ [c]	20.7/25.3	21.3/24.4
RMS deviations from ideal geometry		
Bond length (Å)	0.0066	0.0058
Bond angle (°)	1.25	1.17
Average B-factors (Å^2)	38.0	41.7

[a] $R_{merge} = \sum_h \sum_i |I(h)_i - \langle I(h) \rangle| / \sum_h \sum_i I(h)_i$.

[b] $R_{work} = \Sigma h|F(h)_{calcd} - F(h)_{obsd}|/\Sigma h F(h)_{obsd}$, where $F(h)_{calcd}$ and $F(h)_{obsd}$ were the refined calculated and observed structure factors, respectively.

[c] R_{free} was calculated for a randomly selected 3.5% (PTP1B•LZP25) and 4.9% (PTP1B•LZP6) of the reflections that were omitted from refinement.

Table 4

IC_{50} values of LZP6 for wild-type and mutant PTP1B

PTP1B	**IC_{50}, μM**
WT	16±2
R47V	16.4±1.1
F182A	58.7±2.5
F196A	12.6±1.5
F280A	11.8±0.8
Q262A	55.6±2.9
T263A	37.6±2.0

All measurements were made using *p*NPP as a substrate at pH 7.0, 25 °C, and I=0.15 M.

Table 5

Selectivity of LZP25 and LZP6 against a Panel of PTPs

PTPs	**IC_{50} for LZP25 (μM)**	**IC_{50} for LZP6 (μM)**
PTP1B	20 ± 5	16 ± 2
HePTP	87 ± 6	72 ± 4
SHP2	85 ± 8	58 ± 4
Lyp	73 ± 20	70 ± 24
VHR	113 ± 6	108 ± 6
LAR	No inh. at 100 μM	No inh. at 100 μM
PTPα	No inh. at 100 μM	No inh. at 100 μM

All measurements were made using *p*NPP as a substrate at pH 7.0, 25 °C, and I=0.15 M.